LPR: A CT and MR-Compatible Puncture Robot to Enhance Accuracy and Safety of Image-Guided Interventions

Nabil Zemiti, Ivan Bricault, Céline Fouard, Bénédicte Sanchez, and Philippe Cinquin

***Abstract*—Image-guided percutaneous interventions are common procedures used for diagnosis or therapeutic purposes. The clinical demand for such interventions is growing since they are minimally invasive. To increase the quality of the operations and provide optimal accuracy and safety to patients, puncture robots may be very helpful. This paper presents a new robotic architecture designed to perform abdominal and thoracic punctures under computer tomography (CT) or MRI guidance. Innovations concerning the robotic architecture, materials, and energy sources are described. Segmentation and registration algorithms have been developed to localize the robot on images coming from CT or MRI devices, and a specific control loop is used to verify the movements and the positioning of the robot. The results of the initial experiments made under CT and MRI environments are presented.**

***Index Terms*—Computer-assisted medical interventions (CAMIs), interventional radiology, localization, magnetic resonance (MR) compatibility, registration, segmentation.**

I. Introduction

In THE interventional radiology field, image-guided percutaneous interventions are common procedures used for diagnosis or therapeutic purposes. Biopsies, abscess drainages, or tumor ablations can be performed percutaneously. The clinical demand for such interventions is growing since they are minimally invasive, and they are often able to prevent the need for a surgical intervention.

The first step in interventional radiology is the puncture of a target, which can be an anatomical structure or a tumor, and whose diameter is generally 1 cm or greater, the dimension considered as clinically significant. These percutaneous punctures can be complicated procedures. The needle insertion is most often controlled with computer tomography (CT), but the planned trajectory can be particularly difficult to implement and to track by the radiologist on CT images when the needle is not aligned with a simple direction of the image plane. Indeed, tilted insertion paths are sometimes advised in order to avoid organs or ribs. Several attempts may be necessary to reach the target, causing a loss of time and more traumas than expected to the patient. Moreover, both radiologist and patient are exposed to X-rays when CT is used to guide the puncture process in real time.

Fig. 1. Photograph of the LPR robot on patient inside MRI device.

As compared to CT, MRI is a promising nonirradiating imaging modality for the real-time control of a puncture, but specific constraints apply in an MRI environment, in particular, because of the magnetic field and because of the limited access to the patient allowed by traditional closed magnetic resonance (MR) devices; the diameter of the bore does not exceed 60 cm, a space that is also occupied by the patient.

The use of robots for surgical interventions is an approach that has been proven to increase the quality of operations and to establish new types of surgical procedures [1], [2]. In the context of interventional radiology, puncture robots may be very helpful. They have the potential to work within CT or MRI, and to decrease the intervention duration while providing optimal accuracy and safety to patients.

These factors have motivated our research in the development of a new lightweight robot for abdominal and thoracic percutaneous procedures that is compatible with CT, open MR, and closed MR. Our aim is to control in real time the initial positioning of the needle and the puncture movement itself. Thus, the robot has to be able to operate alone, but with remote medical supervision, inside the CT or MR guidance imaging device.

This robot (see Fig. 1), named light puncture robot (LPR), has an original compact body-supported architecture, which is naturally able to follow the patient body surface respiratory movements. It is entirely made of plastic and uses MR-compatible

Manuscript received November 15, 2007; revised February 20, 2008. Recommended by Guest Editor N. Tsekos.

N. Zemiti, C. Fouard, B. Sanchez, and P. Cinquin are with the Computer-Assisted Medical Interventions Team, Techniques de l'Ingénierie Médicale et de la Complexité-Informatique, Mathématiques et Applications de Grenoble (TIMC-IMAG) Laboratory, IN3S, 38706 La Tronche Cedex, France (e-mail: Nabil.Zemiti@imag.fr; Celine.Fouard@imag.fr; Benedicte.Sanchez@imag.fr; Philippe.Cinquin@imag.fr).

I. Bricault is with the Computer-Assisted Medical Interventions Team, Techniques de l'Ingénierie Médicale et de la Complexité-Informatique, Mathématiques et Applications de Grenoble (TIMC-IMAG) Laboratory, IN3S, 38706 La Tronche Cedex, France, and also with the Medical Imaging Department, Grenoble University Hospital, 38043 Grenoble Cedex, France (e-mail: Ivan.Bricault@imag.fr).

Digital Object Identifier 10.1109/TMECH.2008.924045

pneumatic actuators powered by compressed air. It is localized via an image-based control using a localization device that is totally integrated to the robot. The physician is also included in the control loop since he/she selects the target and the entry point and supervises the whole process.

A prior version of the LPR robot with first *in vivo* experiments performed under CT scanner have been presented in [3]. Even though this robot version was designed to be MR compatible, it did not respect the MRI bore space requirements. In Section III, we present a new compact needle-holder architecture solving this problem. The robot position control procedure that have been previously developed for CT applications [3], [4] has been adapted for MRI applications and is described in Section IV. Experimental evidence and MR-compatibility tests of the system are presented in Section V. A discussion of the results and further directions for research are given in Section VI.

II. Related Work

Since the early 1990s, more than 159 surgical robotic systems have been developed [2]. In the field of MRI interventional robotics, there exists, to our knowledge, only one commercial MRI-compatible system: the Innomotion robot for percutaneous interventions (Innomedic, Germany, `www.innomedic.de`).

Innomotion is a pneumatic robot fully MR compatible developed to provide precise and reproducible needle positioning inside the magnet [5]. It consists of a 6-DoF robot arm that is attached to a 260° arch mounted to the patient table and can be passively prepositioned according to the region of interest (RoI). The robot position control is based on optical fiber position encoders. The kinematics of the device has been optimized for use in close MRI bore and CT scanners. However, the current version of the system provides only position guidance, i.e., the robot moves automatically the needle to the desired insertion point with the desired orientation, and then, the physician advances the needle manually.

For closed bore MRI interventions, it is difficult to advance the needle manually inside the magnet bore. The patient table has to be moved outside the bore to perform the puncture correctly.

However, if the robot is mounted to the table and not body supported by the patient (which is the case of the Innomotion system), any nonintentional movement of the patient during the table displacement may make changes in the planned needle trajectory with respect to the desired one. Consequently, as we cannot have real-time needle guidance outside the MR bore, such robot architecture may not be robust with respect to patient movement and might cause injury to the patient when delicate organs are considered.

Other MRI interventional robots are currently available at research laboratories. The major challenge for the development of these systems is the MR compatibility [6]–[8].

Several research groups have developed MR-compatible robots actuated by ultrasonic motors. Although these actuators are not affected by the magnetic field, their housing contain conductive material that result in substantial image artifacts if placed just near the MR magnet [9]. Shielding or placing these motors inside a Faraday cage does not eliminate the artifacts [10]. Such actuators could be placed far away from the MR magnet as in [11] and [12], where MRI-compatible robots for biopsy and therapeutic interventions in the breast were presented, and in [13], where the design of a novel MR-compatible manipulator for prostate intervention was detailed. One can note that, for such specific clinical applications, it is possible to have long distance interaction between the control unit (ultrasonic motors) outside the MRI magnet and the patient inside the magnet. However, in the general case, this configuration is not suitable since it decreases the rigidity of the system, as it has been emphasized in [14].

Electrostatic motors could also be used within an MR environment. As compared to ultrasonic motors, they operate at lower frequencies (typically up to 1 kHz) and at lower currents, so they should less interfere with MRI imaging [15]. However, as the electrostatic motor is driven by a three-phase ac high-voltage source (2 kV peak to peak), it still requires developments on the power electronics to be used in the operation room.

Alternatively to ultrasonic or electrostatic motors, a hydrostatic transmission approach is proposed in [9] and a 1-DoF MRI and functional MRI-compatible robot is presented. The concept is based on a telemanipulator system with a mechanical transmission between the master and the slave. The master part of the robot (conventional actuator) that contains the interfering or sensitive components is placed outside the magnet shield in the control room. A hydrostatic connection is used to transmit force and motion to an MR-compatible slave placed next to or inside the MR scanner. For position control, the robot uses a home-made fiberoptic displacement sensor. The main feature of this system is that it is equipped with a force sensor, based on reflected light intensity measurement over optical fibers that measures interaction forces with the human subject.

A new robot, named MrBot [5], was recently developed at The Johns Hopkins University. It uses a new type of pneumatic step motors (the PneuStep) [16] specifically designed for MRI application. The robot is customized for transperineal needle insertion for prostate gland under either open- or closed-bore MRI scanners. It is exclusively constructed of nonmagnetic and dielectric materials such as plastics, ceramics, and rubbers, and is electricity free. Fiber-optic encoding is used for position feedback, so that all electric components are distally located outside the MRI shield.

It is shown that devices constructed in [17] using binary polymer-based actuators, called electrostrictive polymer actuators (EPAMs), are able to function within the MRI without degrading its imaging performance. The binary nature of these actuators eliminates the need for feedback sensors for motion control. Their construction is fundamentally inexpensive and simple. They can be constructed essentially from plastic, making their potential cost low enough to be disposable. This attractive approach remains to be explored further.

For further details about MR-compatible robots and mechatronic devices, the reader can refer to [18], [19], and the references within.

III. Robot Description and Specifications

The LPR architecture is mainly based on the prior works done at the Techniques de l'Ingénierie Médicale et de la Complexité

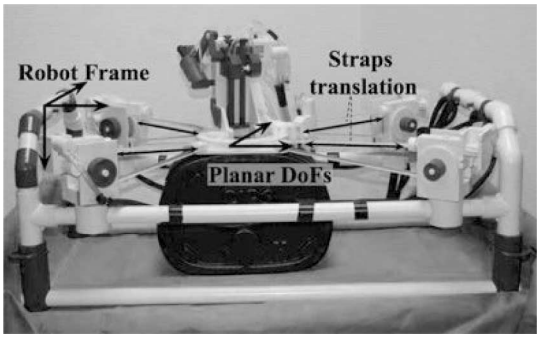

Fig. 2. LPR entire robot placed on an abdominal phantom.

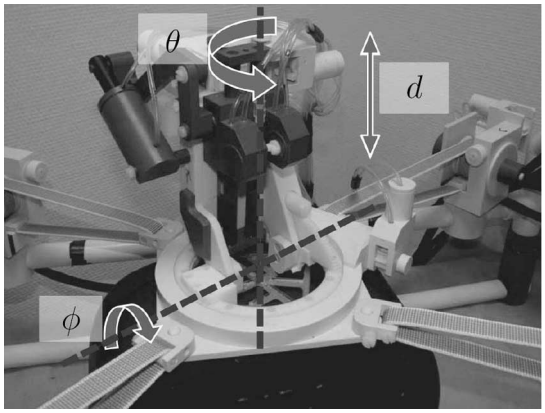

Fig. 3. Needle-holder DoFs.

(TIMC) Laboratory on the tele-echography robot [20] and the light endoscopy robot [21], [22]. It is lightweight (1 kg), compact (15 cm × 18 cm), and its installation is particularly simple, so that the necessary setup time is greatly reduced.

As shown in Figs. 1 and 2, the main feature of this robot is its original body-supported architecture [23], which suppresses the risk of accidental trauma on the patient's body by robot or needle parts. Indeed, since the robot follows the patient's abdomen/thorax surface, this provides an intrinsic compensation for some physiological or unexpected movements of the patient.

This concept of placing the robot on the patient has been also chosen in [24] and [25] for endoscopic surgery (the MC^2E robot), in [26] for percutaneous cholecystostomy interventions (the UMI system), and in [27] for CT-guided percutaneous interventions (the CT-Bot system). For the sake of clarity, we resume here the robot architecture presented in [3].

The LPR possesses five DoFs and is composed of two parts. The main part, the needle-holder that is laid directly on the patient's body, provides three DoFs (see Fig. 3): a translation $d \in [0\ 9\,\text{cm}]$ along the needle axis, a rotation $\theta \in [0\ 2\pi]$ with respect to the robot's platform and around an axis normal to the patient's body, and an inclination $\phi \in [-\pi/18\ \pi/3]$ of the needle-holder with respect to the robot's base.

The second part of the robot is composed of a support frame and four actuators that provide the two remaining DoFs, i.e., the translation over the patient's body that gives natural standoff and orientation to the robot (see Fig. 2). This movement is done,

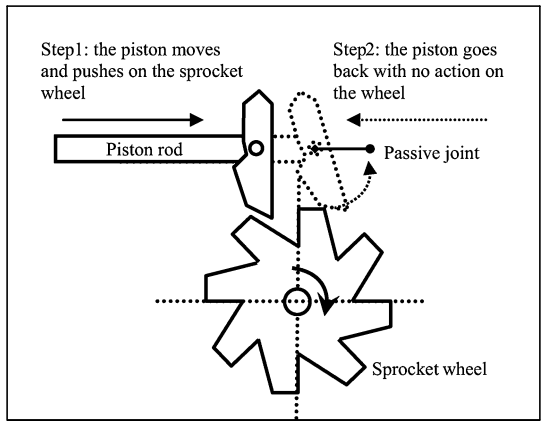

Fig. 4. Principle of the pneumatic actuator for controlling the LPR movement.

thanks to four straps. The architecture of the support frame offers the possibility of making a height adjustment of 10 cm in order to adapt the robot to the patient's corpulence and to the imaging system size.

The LPR is made of plastic materials (nylon, delrin, and epoxy) that have been chosen in order to ensure MR compatibility with a null signal in the MR images and a minimum of artifacts under CT environment [6], [10]. In order to be totally compatible with the MR environment, compressed air is used as an energy source. The robot controller and air compressor are linked to the actuators by 7-m-long plastic tubes, allowing them to be placed outside the MR room, beyond the magnetic hazard zone.

A new and original way to use pneumatic actuators, based on clock-making principles, was developed. Each actuator can achieve bidirectional movement, thanks to two sets of pistons, cylinders, and sprocket wheel, one set for each movement direction. On each side of the cylinder, one air inlet brings the compressed air (4 bar pressure) to the piston. Air is alternatively injected in each cylinder compartment to achieve the piston movement. The first step to move the actuator in the chosen direction consists in moving the corresponding piston and pushing the associated sprocket wheel by one increment. The second step consists in making this piston returning back without any action on the wheel through the use of a passive joint (see Fig. 4).

This incremental movement is rated at a maximum frequency of three impulses per second. A worm gear is assembled to the sprocket wheels' axis and works with its corresponding gear (see Fig. 5). This setup allows the user to block the robot in a certain position when the pistons are not solicited.

Each of the four actuators performing the translation motion of the needle-holder over the patient's body has a pulley that allows the strap to be entangled/disentangled (see Fig. 5). Each strap is bounded to the needle-holder platform on one side and to the pulley on the other side.

When the robot is installed on the patient, these translation actuators can be disengaged in order to fix the straps stretch (thus the pressure exerted on the patient) and perform a manual prepositioning of the needle-holder on the patient's body.

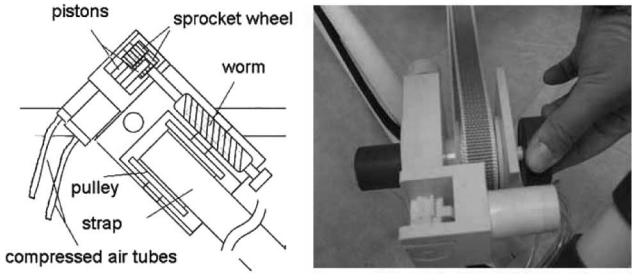

Fig. 5. LPR translation principle.

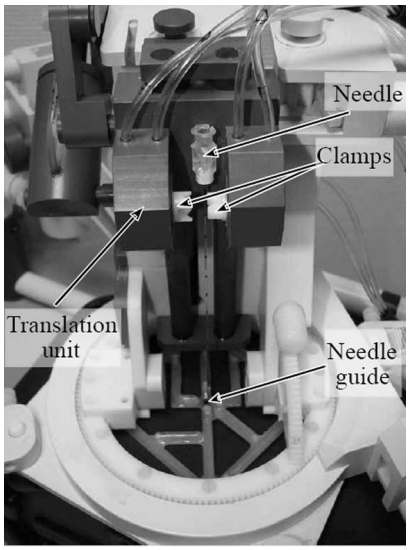

Fig. 6. Needle-holder puncture part.

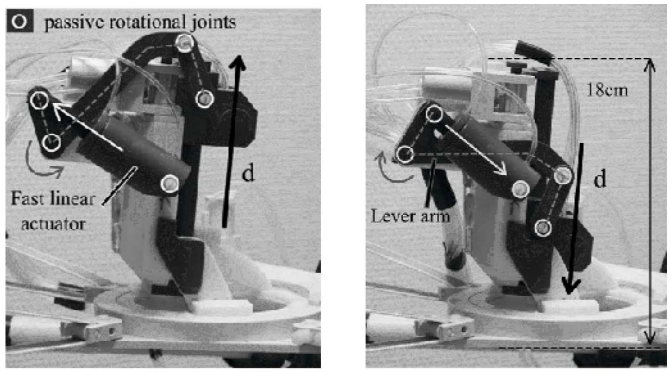

(a) (b)

Fig. 7. Needle extracting and inserting principle. (a) Needle extracted. (b) Needle inserted.

In practice, when specifying a desired entry point, the robot controller computes the desired length of each strap that shall translate the needle-holder platform from its actual position to the desired one.

Knowing the desired length of each strap and their current values (the initial length before staring the movement), one can easily compute the number of increments to realize per piston, i.e., the number of air impulses to send that should achieve the desired translation. The air impulses are sent to the actuators at different frequencies to coordinate the movement of the four straps.

Note that this translation command algorithm works under the assumption that the needle-holder platform translates over a flat surface. This assumption is true in practice, since the operator has to manually preposition the needle-holder near to the planned entry point when the robot is installed on the patient. In this case, the patient's body curvature is negligible with respect to the travel distance. The surface over which the robot will translate can thus be easily approximated to a plane. Moreover, by reducing the travel distance, one reduces also the overall operation duration and limits the positioning error.

The needle-holder puncture part, depicted in Fig. 6, includes clamps used to grasp the needle, and a translation unit that penetrates/extracts the needle into/from the skin or organs walls.

The translation unit is moved up/down, thanks to a fast linear pneumatic actuator that pushes on a rigid lever arm transmission (a "*parrot-nose like*" arm) combined with five passive rotational joints. Fig. 7 illustrates the needle inserting and extracting principle where the lever arm is emphasized with the dotted line. Thanks to this laterally deported actuation, the translation unit is able to perform a fast puncture in a single motion (above 9 cm/s) to perforate the skin or organs walls.

To guarantee that the puncture movement will be straight, the needle is inserted through a guide placed at the center of the robot base.

The puncture depth (i.e., the distance from the entry point to the targeted point) is controlled via a thrust bearing that stops the motion of the fast linear actuator. The locations of the entry point and the target point have to be specified by the physician during the path planning, defining thus the desired position of the thrust bearing. This position can be precisely controlled with a resolution of 0.16 mm using a slow pneumatic actuator based on clock-making principles running at three impulses per second (piston + sprocket wheel).

If the target distance from the entry point is greater than the needle-holder stroke (9 cm), the robot can perform a deeper insertion by releasing the needle and grasping it higher. When it is released by the clamps, the needle can follow the movements of the patient's target organ, thus avoiding injuries. This approach also offers the possibility of performing the needle insertion in several steps, identically to the way the physician often works manually. Between each new motion step, the physician has the opportunity to verify, and eventually to update, the desired needle trajectory.

Ideally, the robot might automatically grasp the needle again after it has been released. To do so, we can ask the patient to reproduce identical apneas before each needle regrasping, which is supposed to replace the needle at the same position where it was released just before, i.e., at the center of the clamping mechanism. However, in practice, one cannot guarantee the success of this operation. In fact, nonreproducible apnea can occur and results in the needle moving away from the clamping mechanism. Consequently, physician supervision is mandatory

TABLE I
LPR SPECIFICATIONS

Description	Value
Air pressure	4bar
Needle driver max. force capability	80N
Needle penetration velocity	9cm/s
Actuators max. frequency (impulses per second)	3Hz
Translational resolution (patient body plan)	0.14mm/impulse
Needle penetration resolution (incremental positioning of the thrust bearing)	0.16mm/impulse
Base rotation resolution	$0.3°/\text{impulse}$
Needle orientation resolution	$0.375°/\text{impulse}$
Base rotation range	$\theta \in [0 \;\; 2\pi]$
Needle orientation range	$\phi \in [-\pi/18 \;\; \pi/3]$

when performing deeper insertion by releasing the needle and grasping it higher.

Although the insertion velocity and force cannot be controlled with the current needle-holder, this system is clinically adequate for percutaneous interventions, since it is possible to precisely control the needle penetration depth, and to produce a sufficient insertion force to safely penetrate the patient skin and tissues. The force and velocity capabilities of the LPR insertion device (80 N for the force and 9 cm/s for the velocity) are satisfactory regarding to the stiffness of the patient skin and tissues and also to the duration of the patient apnea, which should not exceed 10 s for optimal patient comfort. The overall robot specifications are summarized in Table I.

IV. ROBOT POSITION CONTROL

An important issue for robot guidance is the precise localization of the end effector in the intraoperative space. To do so, and as an alternative to conventional position encoders, localization modules are usually placed on the robot or its end-effector [27], [28]. Here, we also designed a specific localization device that can be used to compute the LPR position and orientation (the three translational and rotational DoFs) according to the CT/MR reference.

This localization device is a square frame made of epoxy resin ensuring CT visibility (see Fig. 8). For MRI visibility, glass tubes of 2.4 mm diameter filled with dilute gadolinium-chelate solution[1] have been pasted on the localization device surface. A concentration of 2 mmol/L has been chosen to ensure the fiducial visibility with good signal intensity (SI) under both T1- and T2-weighted MR-acquisition sequences [29]. In order to avoid any liquid evaporation and MRI signal discontinuity caused by the presence of air bubbles within the tubes, the gadolinium solution has been jellied by the use of an agar–agar powder (powder used as gelling and stabilizing agent in food) and the glass tubes have been sealed with a waterproof and tight silicone glue.

[1]GADOTERIC acid, DOTAREM, Guerbert Laboratories.

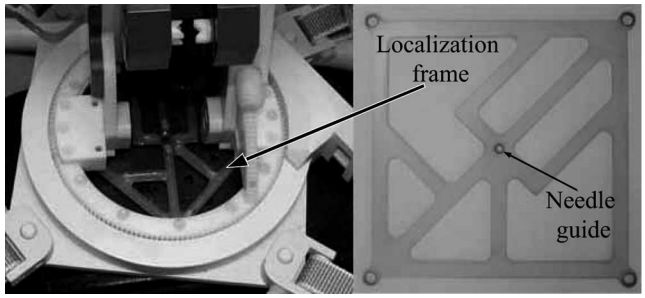

Fig. 8. Localization device.

This localization device is rigidly fastened with screws to the proximal end of the rotating base of the robot so that it is totally integrated into the needle-holder architecture.

In the current robot design, this localization device does not follow the inclination movement of the needle-holder, i.e., this fiducial does not give information about the needle inclination. To do so, the alternative adopted solution is to place the robot, at the beginning of each experiment, in an initial configuration corresponding to a $90°$ inclination of the needle with respect to the localization device. Then, the control system relies on this *a priori* knowledge of the initial position to keep track of the current needle inclination after each inclination movement command. Automatic image-based computation of the needle-holder inclination is to be considered in the ongoing research.

Each time we want to know the robot position to verify if it is correct, we have to acquire a set of images. Then, the images are automatically processed in order to detect the localization device and find the current orientation of the robot and the entry point. These images also allow the radiologist to confirm the adequate progression of the procedure.

LPR localization involves image processing algorithms that have been developed and previously validated on CT images [3], [4]. These algorithms, described hereafter, have been successfully adapted and validated on MR *in vivo* images acquired with a Philips Achieva 1.5 T MR device using a standard breath hold THRIVE 3-D Gradient-Echo T1-weighted[2] sequence (15 s acquisition duration) and an RF body coil [see Fig. 9(a)].

The first step of the image processing is a smoothing that enhances the image quality. A mask containing the patient's abdomen is then created using an adequate thresholding and mathematical morphology operations. This mask is subtracted to initial image resulting in a large majority of localization device points for a minority of points of other objects. Finally, after a last thresholding, all the regions of the resulting binary image are labeled in connected components, and *a priori* knowledge of the localization device geometry is applied in order to conserve only the points of interest [see Fig. 9(b)]. The whole image processing takes less than 30 s to be implemented.

Ongoing research is done on implementing a 3-D chamfer-matching algorithm [30] in order to register the segmented cloud of points with the 3-D model of the localization device (see

[2](Repetition time (TR)/echo time (TE): 4.04 ms/1.97 ms, flip angle: $10°$, slice thickness: 6 mm, echo train length: 60, field of view (FOV) 395 mm, resolution: 256×256).

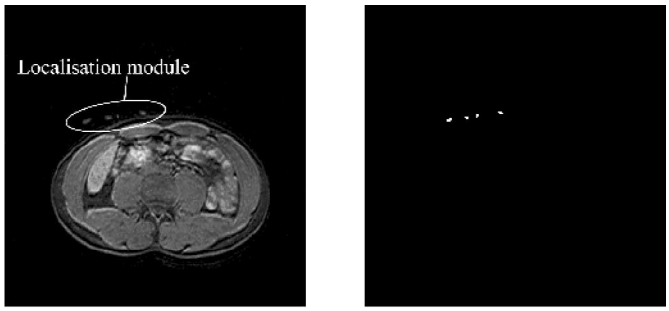

(a) (b)

Fig. 9. Localization module segmentation from MR images. (a) MR image acquired during *in vivo* experiment on a healthy volunteer's abdomen: the LPR structure generates no signal, only the patient's abdomen and the localization module are visible. (b) Thresholding step extracts parts from the localization module from the rest of the patient's abdomen. Geometric criteria succeed in selecting only parts from the localization module.

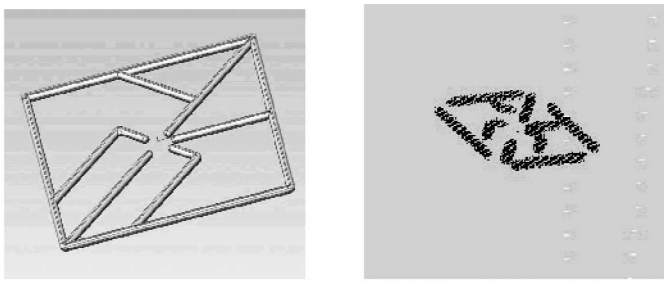

(a) (b)

Fig. 10. Localization module 3-D model and segmentation result. (a) Localization device 3-D model. (b) Cloud of points resulting from the localization module segmentation algorithm.

Fig. 10). As a result, the registration parameters (rotation and translation) should give the position and orientation of the localization device, i.e., the position of the robot and of the needle tip since the geometric relationships between all these elements are precisely known.

V. Experimental Results

A. Robot Implementation

To interact with the system, we developed a human–machine interface, named LPRManager which consists of three subsystems: a robot controller, an MR/CT image processor, and a graphical user interface. It runs on its own laptop (Pentium 4, 2.4 GHz, 512 Mo RAM) running under a Windows XP operating system (OS).

1) *Robot controller:* A Personal Computer Memory Card International Association (PCMCIA) DIO Card (a DAQCard-DIO24 from National Instrument) is used to communicate with the robot controller (valves, switches, etc.) that actuates the robot pneumatic pistons. To do so, the DIO card sends a 5 V signal to move the piston front and a 0-V signal to move the piston back. This DIO card allows to control the pistons simultaneously and/or independently, which is an interesting feature for the actuators movement coordination.
2) *Image processor:* To determine the robot position on the CT/MR images, as detailed in Section IV, we use the Insight ToolKit (ITK) software library on 3-D digital imaging and communications in medicine (DICOM) images obtained through the network by a DICOM query/retrieve service class (SCU/SCP) protocol.
3) *GUI:* The GUI is designed with the WxWidgets and OpenGL libraries to be able to display DICOM volume images on arbitrary cut planes.

The system is implemented as follows.

1) The patient is installed on the imaging device bed and the robot frame is positioned on the patient.
2) The needle-holder part is manually prepositioned on the patient's abdomen near the expected puncture point given by the preoperative planning.
3) A first volume image containing both the patient-targeted organs and the robot-localization device is acquired (with a standard procedure), and then, transfered through the network to the LPRManager computer. Note that we use standard CT and MRI sequences (no specific acquisition sequences has been developed) in which the patient has to hold his/her breath during approximately 15 s. The only constraint to localize the robot is that the obtained images resolution is fine enough to precisely describe the robot localization device.
4) From the scanner's control room, the physician uses the GUI to review the acquired slices showing the patient anatomy (and the robot localization) and chooses, by a simple mouse click, the target point within the patient's body and the needle entry point that determines the desired trajectory.
5) The LPRManager performs a registration between the DICOM patient image and the robot models as described in Section IV. The operator can confirm or correct this registration.
6) The LPRManager computes the displacement between the robot's current and desired position. The operator can then adjust, and/or confirm, and launch the displacement order.
7) The LPRManager computes and sends the low-level commands to the robot actuators.
8) A second volume image containing the robot-localization device and the planned needle trajectory is acquired to verify the actual robot position.
9) If necessary, these five last steps can be iterated in order to ensure optimal accuracy.
10) The operator gives the puncture movement order to the robot. Robot clamps can release the needle once its tip has been inserted into the target.

B. Accuracy Experiment

Accuracy experiments were performed on a plane surface inside a CT scanner. They consisted in moving the robot to a particular position/inclination, and measuring its positioning accuracy with a CT acquisition control. These experiments were performed 15 times. For each experience, the robot was moved between different initial and final positions/inclinations.

For the robot base rotation and needle-holder inclination tests, the expected angles were obtained with an angular error less than 1°. Concerning the translation tests, we have obtained a strap-based translation accuracy of 5% of the displacement d; for instance, with $d = 20$ mm, the maximum error was 1 mm. Additionally, to evaluate the repeatability of the translation, each move was achieved back and forth four times; the same translation was achieved almost identically with a maximum variability of 0.5 mm.

Experiments on a phantom have shown the capacity of LPR to extract its exact position using the localization device and image-processing algorithms, and to reach its target with millimeter accuracy [3]. These experiments consisted in trying to reach a target from an unknown position and orientation of the robot, with a CT images control. We used a 60 cm $\times$ 34 cm $\times$ 27 cm foam rubber block in which we inserted a polyether–cetone disc with a 1 cm hole as a target.

In these experiments, the distance between the tip of the needle and the target point (i.e., the center of the polyether–cetone disc) was smaller than 2 mm (error range = 0.3–1.8 mm), so that the clinically significant 1 cm central hole target was correctly punctured.

Additionnally, initial *in vivo* animal experiments on four pigs have been conducted within a CT environment [3]. These preliminary *in vivo* experiments have demonstrated the feasibility of the LPR concept in clinical conditions. During these experiments, we have noted that the robot had no difficulty in getting a rather large 17-gauge needle to penetrate pig skin, even if the pig's tissue stiffness is higher than the humans' one. The resulting accuracies were measured within the range of 1 cm. This range can be considered as clinically acceptable, since any lesion measuring less than 1 cm in a patient is generally followed up by imaging; a more invasive decision such as biopsy or ablation is rarely taken unless the lesion gets larger than 1 cm.

C. MR-Compatibility Experiment

The LPR's MR compatibility has been assessed on a clinical MR equipment (Achieva 1.5 T, Philips Medical Systems). Qualitative compatibility tests were conduced first without any patient, second, while imaging the robot placed over the abdomen of a volunteer (see Fig. 1). Various clinical MR sequences, routinely used for abdominal imaging, have been tested: standard [fast field echo (FFE)] and 3-D volume interpolated [T1-weighted high resolution isotropic volume examination (THRIVE)] breath-hold gradient-echo T1-weighted acquisitions, breath-hold, and respiratory-triggered turbo spin-echo (TSE) T2-weighted acquisitions.In every case and as expected, LPR plastic components generated no signal in the images and caused no artifacts on the adjacent abdominal organs.

Additionally, quantitative evaluation tests based on SNR measurement were conduced on a copper sulfate ($CuSO_4$) cylindrical phantom bottle.

The SNR was calculated by dividing the mean SI of an RoI by the standard deviation (SD) of the noise calculated from an RoI placed in an empty space [31]. Namely, the SI is calculated from an RoI that corresponds to a small area of the phantom

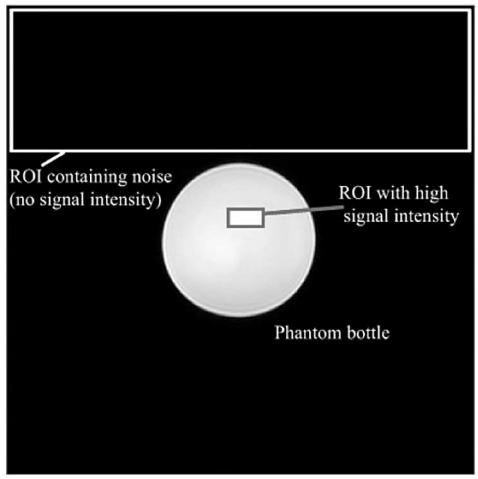

Fig. 11. SNR calculation principle.

TABLE II
SNR OF PHANTOM IMAGES WITH AND WITHOUT LPR IN PLACE

	No device in place (reference value)	LPR in place
T2-weighted seq.	446.2 ($\pm$57.5)	402.7 ($\pm$77.4)
T1-weighted seq.	179 ($\pm$64.5)	161.7 ($\pm$59.3)

that have a high SI. The SD of the noise is calculated from the biggest empty region of the image that contains no signal (see Fig. 11).

In a first set of experiments, the SNR was calculated from a high-quality image without the robot in place. This gives rise to a high SNR value that represents the SNR reference value. In a second set of experiments, the SNR was calculated from an image collected with the LPR placed on the phantom bottle. These experiments were conduced using an RF body coil with both Turbo spin-echo T2-weighted[3] and THRIVE 3-D gradient-echo T1-weighted[4] sequences and repeated for each image of the acquired volume so that 25 SNR measurements (respectively, 65) for the T2-weighted sequence (respectively, for the T1-weighted sequence) were computed.

The SNR measurement results are summarized in Table II where the mean SNR value for each sequence is given with its corresponding SD value between the brackets. These results show that the LPR did not produce significant changes in the SNR values, validating thus the MR compatibility of our device.

VI. DISCUSSION AND CONCLUSION

In this paper, we have presented a new lightweight and compact CT an MR-compatible puncture robot, named LPR. The system installation and its clinical implementation are particularly simple, and the necessary setup time and the operation duration are greatly reduced. To install the robot, one had just to correctly place the robot frame on the patient and preposition the needle-holder platform near the planned entry point.

[3](TR/TE: 1600 ms/70 ms, flip angle: 90°, slice thickness: 7 mm, echo train length: 25, FOV 405 mm, resolution: 512×512).

[4](TR/TE: 4.03 ms/1.96 ms, flip angle: 10°, slice thickness: 6 mm, echo train length: 60, FOV 395 mm, resolution: 256×256).

As compared to the other existing puncture robot, the LPR is both MR and CT compatible. This allows to transform any conventional CT and closed MR scanner into an image-guided interventional device without performing any adaptation on the system. In order to be totally compatible with the MR environment, the pneumatic actuation has been chosen, and a new and original way to use pneumatic actuators, based on clock-making principles, was developed. Note that the same solution has also been chosen for the MrBot actuation (the PneuStep) [16].

The LPR robot has a body-supported architecture that suppresses the risk of accidental trauma on the patient's body by robot or needle parts. To our knowledge, there exists no MR-compatible system that proposes this architecture. The LPR needle-holder platform can follow the patient's abdomen/thorax surface and intrinsically compensates some physiological or unexpected movements of the patient. However, one had to emphasize that during the puncture step itself, i.e., just before the needle is moved toward its internal target, an apnea identical to the one performed during the last image acquisition is required from the patient. If not, the external body movements due to respiration may not be correlated with internal organ breathing movements and may interfere with the planned needle trajectory.

Contrary to other MR-compatible anthropomorphic puncture robots with a plastic long arm and a deported actuation, in the case of a modular and very compact body-supported system such as the LPR, the rigidity of the overall system is not a major concern. Indeed, since the needle-holder platform is laid directly on the patient's body and is translated at slow rates (quasi-static movement) over this latter using stretched straps, positioning errors due to the system flexibility (lever arm effects, oscillated movements, inertial effects, etc.) are not encountered.

The translation accuracy experiments of the robot over patient body surface has proved to be very satisfactory over small distances (less than 30 mm). Above this limit, the displacement is not as accurate; this is the counterpart of the body-supported strap-based translation design, where the robot is partially free to adjust its motion to the underlying surface. Nevertheless, since the loop is closed by CT/MR image acquisition and supervised by the physician, it is always possible to reach an excellent accuracy, as the physician can refine the robot position with an iterated translation. Ultimately, the final translation can always be set to be less than 30 mm. Under such conditions, experiments gave very promising results. Accuracy for orientation and inclination was proven to be under 1°, and accuracy for the final puncture on a phantom with a depth up to 6 cm was less than 2 mm.

Preliminary *in vivo* experiments also gave results compatible with clinical applications, yet we can note that our *in vivo* experimental setting was particularly challenging for the following reasons.

1) Animal abdomens were significantly smaller than a usual human body; the robot had to translate over a nonflat surface with exaggerated curvature. Thus, the translation was less predictable. In this context, additional iterations can be useful to reach an optimized final puncture position.
2) The robot might also have been less stable in the small animal's abdomen than in a flatter surface, even though the LPR weight, the strap tension, the contact between skin surface, and robot base allowed no visually detectable robot instability during positioning or puncture.
3) Last but not least, it was not possible to obtain an apnea from the animals during our *in vivo* experiments. Thus, the larger part of the final puncture inaccuracy can be assumed to be due to respiratory motion. These points will deserve further *in vivo* evaluations.

Segmentation and registration algorithms are currently based on image data acquired in a small volume that includes the localization device with postmotion processing. Further work will be done in order to provide a fast closed control loop, in real-time during robot motion, based on a single slice image acquisition.

Algorithms used during the LPR localization process have initially been developed with CT images. However, thanks to materials employed to construct the robot, its compact architecture, and the remote pneumatic energy source used to actuate it, LPR is fully MRI compatible, and image acquisitions with LPR have already been achieved in a clinical closed MRI bore.

Ongoing research is done on adapting the CT segmentation and registration algorithms for MR images. This will allow the first LPR experiments with MRI on healthy volunteers, and will further demonstrate the possibility with LPR to transform a simple CT or closed MR into a real-time controlled interventional imaging device.

Let us note that manipulating and driving a needle inside a closed MRI bore, and in the presence of a corpulent patient inside the bore, imposes a drastic limitation of the workspace [14]. Furthermore, this confined workspace is very dependent upon the needle orientation and the patient size and position. Indeed, during the experiments with the LPR, we have first measured the transversal workspace available between the patient's table and the inner MRI bore surface (a Philips Achieva, 60 cm Ø, 1.5 T) without any patient inside. At the midsagittal plane of the bore, this workspace is maximal and equals ≈ 40 cm. When placing a male subject (1.65 m height and 65 kg weight) inside the MRI bore, the transversal workspace at the midsagittal plane of the bore is reduced to ≈ 22 cm (the distance from the abdomen surface to the inner surface of the MRI bore). Off this midsagittal plane, due to the noncylindrical shape of patient's body, the workspace in an oblique plane can rapidly decrease to become as small as ≈ 15 cm .

However, if this workspace is able to contain the adequate needle chosen for the puncture, the intervention can also be performed using our needle driver under the condition that this latter presents a smaller (or equal) height than the chosen needle. The current prototype almost verifies this condition (18 cm height) and we are now working on the development of a smaller needle driver in which the height (≈ 10) cm will be compatible with the length of most existing biopsy needles.

One can note that MRI scanners are now available with 70 cm bore diameters even though they are not yet commonly distributed. This could allow obese patients to benefit from our system.

An important point to consider when developing a medical device is the possibility of sterilizing the device components in

contact with human body or protecting them with draping. The LPR is made of plastic materials, i.e., thermoinstable components, which cannot support steam sterilization. The alternative widely used solution for sterilizing heat-sensitive medical devices, such as the LPR robot, is the STERRAD sterilization (`http://www.sterrad.com/Products_&_Services/STERRAD/`); a low-temperature (about 45 °C) hydrogen peroxide gas plasma sterilization. This point will deserve further experimental assessment.

REFERENCES

[1] R. H. Taylor and D. Stoianovici, "Medical robotics in computer-integrated surgery," *IEEE Trans. Robot. Autom.*, vol. 19, no. 5, pp. 765–781, Oct. 2003.

[2] P. P. Pott, H.-P. Scharf, and M. L. R. Schwarz, "Today's state of the art of surgical robotics," *J. Comput. Aided Surg.*, vol. 10, no. 2, pp. 101–132, 2005.

[3] I. Bricault, N. Zemiti, E. Jouniaux, C. Fouard, E. Taillant, F. Dorandeu, and Ph. Cinquin, "Light puncture robot for CT and MRI interventions," *IEEE Eng. Med. Biol. Mag.*, vol. 27, no. 3, pp. 42–50, May/Jun. 2008.

[4] E. Taillant, J. Avila-Vilchis, C. Allegrini, I. Bricault, and P. Cinquin, "CT and MR compatible light puncture robot: Architectural design and first experiments," in *Proc. Int. Conf. Med. Image Comput. Comput.-Assisted Intervention*, Sep. 2004, vol. 3216, pp. 145–152.

[5] K. Cleary, A. Melzer, V. Watson, G. Kronreif, and D. Stoianovici, "Interventional robotic systems: Applications and technology state-of-the-art," *Minim. Invasive Ther. Allied Technol.*, vol. 15, no. 2, pp. 101–113, Apr. 2006.

[6] J. F. Schenck, "The role of magnetic susceptibility in magnetic resonance imaging: MRI magnetic compatibility of the first and second kinds," *Med. Phys.*, vol. 23, no. 6, pp. 815–850, Jun. 1996.

[7] K. Chinzei, R. Kikinis, and A. Jolesz, "MR compatibility of mechatronic devices: Design criteria," in *Proc. 2nd Int. Conf. Med. Image Comput. Comput.-Assisted Intervention*, vol. 1679, Sep. 1999, pp. 1020–1031.

[8] K. Chinzei, K. Yoshinaka, and T. Washio, "Numerical simulations and lab tests for design of MR-compatible robots," in *Proc. IEEE Int. Conf. Robot. Autom.*, May 2006, pp. 3819–3824.

[9] R. Gassert, R. Moser, E. Burdet, and H. Bleuler, "MRI/fMRI-compatible robotic system with force feedback for interaction with human motion," *IEEE/ASME Trans. Mechatronics*, vol. 11, no. 2, pp. 216–224, Apr. 2006.

[10] N. V. Tsekos, A. Özcan, and E. Christoforou, "A prototype manipulator for magnetic resonance-guided interventions inside standard cylindrical magnetic resonance imaging scanners," *J. Biomech. Eng.*, vol. 127, no. 6, pp. 972–980, Nov. 2005.

[11] B. T. Larson, N. V. Tsekos, A. Erdman, E. Yacoub, P. Tsekos, and I. Koutlas, "Design of an MRI-compatible robotic stereotactic device for minimally invasive interventions in the breast," *J. Biomech. Eng.*, vol. 126, no. 4, pp. 458–465, Aug. 2004.

[12] H. Fischer, S. Kutter, J. Vagner, A. Felden, S. Pfleiderer, and W. Kaiser, "ROBITOM *II*: Robot for biopsy and therapy of the mamma," in *Proc. IEEE Int. Conf. Syst., Man Cybern.*, Oct. 2004, vol. 3, pp. 2530–2534.

[13] A. Krieger, R. Susil, C. Ménard, J. Coleman, G. Fichtinger, E. Atalar, and L. Whitcomb, "Design of a novel MRI compatible manipulator for image guided prostate interventions," *IEEE Trans. Biomed. Eng.*, vol. 52, no. 2, pp. 306–313, Feb. 2005.

[14] K. Chinzei, N. Hata, A. Jolesz, and R. Kikinis, "Surgical assist robot for the active navigation in the intraoperative MRI: Hardware design issues," in *Proc. IEEE/RSJ Int. Conf. Intell. Robots Syst.*, Oct. 2000, vol. 1, pp. 727–732.

[15] A. Yamamoto, K. Ichiyanagi, T. Higuchi, H. Imamizu, R. Gassert, M. Ingold, L. Sache, and H. Bleuler, "Evaluation of MR-compatibility of electrostatic linear motor," in *Proc. IEEE Int. Conf. Robot. Autom.*, Apr. 2005, pp. 3658–3663.

[16] D. Stoianovici, A. Patriciu, D. Petrisor, D. Mazilu, and L. Kavoussi, "A new type of motor: Pneumatic step motor," *IEEE/ASME Trans. Mechatronics*, vol. 12, no. 1, pp. 98–106, Feb. 2007.

[17] J. Vogan, A. Wingert, J. S. Plante, S. Dubowsky, M. Hafez, D. Kacher, and F. Jolesz, "Manipulation in MRI devices using electrostrictive polymer actuators: With an application to reconfigurable imaging coils," in *Proc. IEEE Int. Conf. Robot. Autom.*, May 2004, vol. 3, pp. 2498–2504.

[18] N. V. Tsekos, A. Khanicheh, E. Christoforou, and C. Mavroidis, "Magnetic resonance-compatible robotic and mechatronics systems for image-guided interventions and rehabilitation: A review study," *Annu. Rev. Biomed. Eng.*, vol. 9, pp. 351–387, Apr. 2007.

[19] N. Yu and R. Riener, "Review on MR-compatible robotic systems," in *Proc. 1st IEEE/RAS–EMBS Int. Conf. Biomed. Robot. Biomechatron. (BioRob)*, Feb. 2006, pp. 661–665.

[20] A. V. Gonzales, J. Troccaz, P. Cinquin, A. Guerraz, F. Pellisier, P. Thorel, B. Tondu, F. Courreges, G. Poisson, M. Althuser, and J.-M. Ayoubi, "Experiments with the TER tele-echography robot," in *Proc. 5th Int. Conf. Med. Image Comput. Comput.-Assisted Intervention*, Sep. 2002, vol. 2488, pp. 138–146.

[21] P. Berkelman, P. Cinquin, J. Troccaz, J. Ayoubi, C. Letoublon, and F. Bouchard, "A compact, compliant laparoscopic endoscope manipulator," in *Proc. IEEE Int. Conf. Robot. Autom.*, May 2002, vol. 2, pp. 1870–1875.

[22] P. Berkelman, E. Boidard, P. Cinquin, and J. Troccaz, "LER: The light endoscope robot," in *Proc. IEEE/RSJ Int. Conf. Intell. Robots Syst.*, Las Vegas, NV, Oct. 2003, vol. 3, pp. 2835–2840.

[23] P. Cinquin, P. Berkelman, A. Jacquet, and J. Arnault, "System for positioning on a patient an observation and/or intervention device", Int. Patent BF 02/05848, May 2003.

[24] N. Zemiti, T. Ortmaier, M. Vitrani, and G. Morel, "A force controlled laparoscopic surgical robot without distal force sensing," in *Proc. Int. Symp. Exp. Robot.*, Singapore, Jun. 2004, pp. 153–163.

[25] N. Zemiti, G. Morel, T. Ortmaier, and N. Bonnet, "Mechatronic design of a new robot for force control in minimally invasive surgery," *IEEE/ASME Trans. Mechatronics*, vol. 12, no. 2, pp. 143–153, Apr. 2007.

[26] J. Hong, T. Dohi, M. Hashizume, K. Konishi, and N. Hata, "An ultrasound-driven needle-insertion robot for percutaneous cholecystostomy," *Phys. Med. Biol.*, vol. 49, no. 3, pp. 441–455, Jan. 2004.

[27] B. Maurin, O. Piccin, B. Bayle, J. Gangloff, M. de Mathelin, L. Soler, and A. Gangi, "A new robotic system for CT-guided percutaneous procedures with haptic feedback," in *Proc. Int. Comput. Assisted Radiol. Surg. Congr.*, Jun. 2004, pp. 515–520.

[28] R. C. Susil, J. H. Anderson, and R. H. Taylor, "A single image registration method for CT guided interventions," in *Proc. 2nd Int. Conf. Med. Image Comput. Comput.-Assisted Intervention*, Sep. 1999, vol. 1679, pp. 798–808.

[29] D. A. May and D. J. Pennington, "Effect of gadolinium concentration on renal signal intensity: An *in vitro* study with a saline bag model," *Radiology*, vol. 216, no. 1, pp. 232–236, 2000.

[30] G. Borgefors, "Hierarchical chamfer matching: A parametric edge matching algorithm," *IEEE Trans. Pattern Anal. Mach. Intell.*, vol. 10, no. 6, pp. 849–865, Nov. 1988.

[31] E. Christoforou, A. Özcan, and N. Tsekos, "Manipulator for magnetic resonance imaging guided interventions: Design, prototype and feasibility," in *Proc. IEEE Int. Conf. Robot. Autom.*, May 2006, pp. 3838–3843.

Nabil Zemiti received the B.Sc. degree in electronics engineering from the University of Science of Algiers (USTHB), Algiers, Algeria, in 2001, the M.Sc. degree in virtual reality and complex systems from the University of Versailles (UVSQ), Versailles, France, in 2002, and the Ph.D. degree in robotics form Paris 6 University, Paris, France, in 2005.

From October 2002 to August 2006, he was a Researcher at the Robotics Laboratory of Paris, Paris 6 University, where he was engaged in research on force-feedback control of medical robots. He is currently a Postdoctoral Fellow at the Techniques de l'Ingénierie Médicale et de la Complexité-Informatique, Mathématiques et Applications de Grenoble (TIMC-IMAG) Laboratory, La Tronche, France, where he is engaged in research on computer-assisted medical interventions and sensor-based control for robotic manipulators.

Ivan Bricault studied sciences and engineering at the Ecole Polytechnique, Paris, France. He received the Ph.D. degree in applied mathematics in 1998, and the M.D. degree in 2002 from the University of Grenoble, Grenoble, France.

He is currently a Radiologist at Grenoble University Hospital, Grenoble, France, specializing in abdominal imaging, and also, an Assistant Professor at Grenoble Medical School, Grenoble. He is also with the Computer-Assisted Medical Interventions research team, Techniques de l'Ingénierie Médicale et de la Complexité-Informatique, Mathématiques et Applications de Grenoble (TIMC-IMAG) Laboratory, La Tronche, France.

Céline Fouard received the M.S. degree in computer science and image analysis from the University of Bordeaux, Bordeaux, France, in 2001, and the Ph.D. degree in computer science and medical image analysis from the University of Nice Sophia Antipolis, Nice, France, in 2005.

During 2005–2006, she worked on image analysis at the Center for Image Analysis, Uppsala University, Uppsala, Sweden, in the field of discrete geometry. She is currently an Assistant Professor at the Techniques de l'Ingénierie Médicale et de la Complexité-Informatique, Mathématiques et Applications de Grenoble (TIMC-IMAG) Laboratory, University of Grenoble, Grenoble, France, where she is involved in teaching computer science and working on computer-assisted medical interventions.

Bénédicte Sanchez received the M.S. degree in image engineering and computer-aided design (CAD) from the University of Grenoble, Grenoble, France, in 2007.

She was with the Computer-Assisted Medical Interventions (CAMI) team of the Techniques de l'Ingénierie Médicale et de la Complexité-Informatique (TIMC) Laboratory, La Tronche, France, where she was engaged in research on the light puncture robot and especially on its localization (image processing). She is currently a Computer Science Engineer at the TIMC Laboratory.

Philippe Cinquin recieved the Ph.D. degree in applied mathematics from the Saint-Etienne and Lyon 1 Universities, France, in 1981.

In 1984, he launched a research team on Computer-Assisted Medical Interventions (CAMI), which led to an innovative approach in surgical practice, due to the introduction of information technology in the operating room, and to four industrial startups. He is a Medical Doctor. He is currently a Professor of Medical Informatics at Grenoble, France, in the Techniques de l'Ingénierie Médicale et de la Complexité-Informatique, Mathématiques et Applications de Grenoble (TIMC-IMAG) Laboratory (TIMC-IMAG), a Research Unit of CNRS and the Université Joseph Fourier, and heads the Center for Technological Innovation at Grenoble's University Hospital.

Dr. Cinquin was the recipient of the 1999 Maurice E. Muller Award for excellence in computer-assisted orthopaedic surgery and the CNRS Silver Medal in 2003.